

Spectroscopic evidence of chirality in tetranuclear Cu(II)-Schiff base complexes, catalytic potential for oxidative kinetic resolution of racemic benzoin

Dipali Sadhukhan , Prithwi Ghosh & Susanta Ghanta

To cite this article: Dipali Sadhukhan , Prithwi Ghosh & Susanta Ghanta (2020): Spectroscopic evidence of chirality in tetranuclear Cu(II)-Schiff base complexes, catalytic potential for oxidative kinetic resolution of racemic benzoin, Inorganic and Nano-Metal Chemistry, DOI: [10.1080/24701556.2020.1852425](https://doi.org/10.1080/24701556.2020.1852425)

To link to this article: <https://doi.org/10.1080/24701556.2020.1852425>



Published online: 10 Dec 2020.



Submit your article to this journal [↗](#)



Article views: 6



View related articles [↗](#)



View Crossmark data [↗](#)



Spectroscopic evidence of chirality in tetranuclear Cu(II)-Schiff base complexes, catalytic potential for oxidative kinetic resolution of racemic benzoin

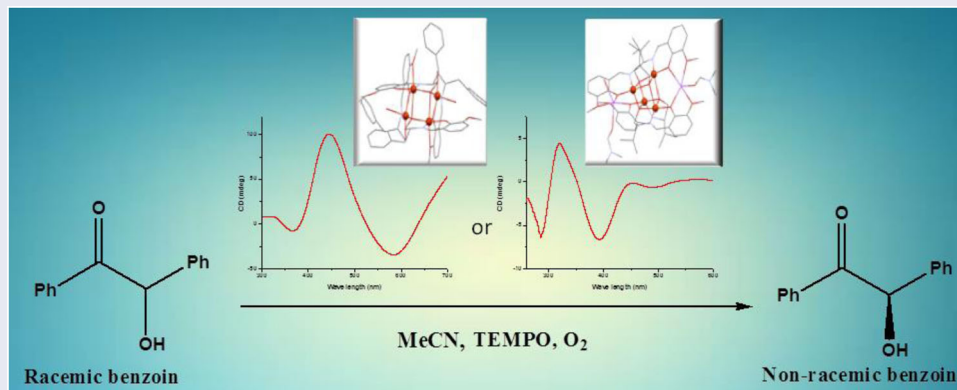
Dipali Sadhukhan^a , Prithwi Ghosh^b and Susanta Ghanta^{a,c}

^aDepartment of Chemistry, Indian Institute of Technology, Kharagpur, West Midnapur, West Bengal, India; ^bDepartment of Botany, Narajole Raj College, Narajole, Paschim Medinipur, West Bengal, India

ABSTRACT

Two chiral Schiff base ligands 2-((1-hydroxy-3-phenylpropan-2-ylidene)methyl)-6-methoxyphenol (**L¹H₂**) and 2-(4-hydroxy-3-isopropylbut-1-enyl)-6-methoxyphenol (**L²H₂**) have been synthesized by the condensation of L-phenylalaninol/L-valinol and o-vanillin (2-hydroxy-3-methoxy benzaldehyde). A tetranuclear homometallic Cu(II) complex [**Cu₄(L¹H)₂(L¹)₂**] (**C1**) and a hexanuclear heterometallic complex [**Cu₄(L²)₄Na₂(DMF)₂(H₂O)] (**C2**) have been synthesized with the ligands. Both the complexes possess cubane like Cu₄O₄ core with interesting structural variations and inherit the chirality of their corresponding ligands. The catalytic potential of the complexes has been explored for the oxidative kinetic resolution of racemic benzoin. The electronic, optical and chiroptical properties of the ligands and the complexes have been studied by DFT and TD-DFT calculations.**

GRAPHICAL ABSTRACT



Two chiral tetranuclear Cu(II) complexes have been synthesized from chiral Schiff base ligands. There are structural, spectroscopic and computational evidence of chirality of the complexes. The complexes show moderate activity toward enantioselective kinetic resolution of racemic benzoin with a maximum of 63% enantiomeric excess.

Abbreviations: OKR: oxidative kinetic resolution; TEMPO: 2,2,6,6-tetramethylpiperidin-1-oxyl; ee: enantiomeric excess; DMF: dimethyl formamide; DFT: density functional theory; TD-DFT: time dependent density functional theory

ARTICLE HISTORY

Received 13 July 2020

Accepted 18 October 2020

KEYWORDS

Chiral complexes; asymmetric catalysts; kinetic resolution; enantioselectivity; TD-DFT calculation

Introduction

In current synthetic chemistry, there is a growing interest of the development of new chiral ligands and their metal complexes as efficient catalysts for asymmetric transformation.^[1] After the pioneering work of Jacobsen and Katsuki^[2] chiral salen-type Schiff base ligands have been extensively used to

synthesize chiral transition metal complexes, excellent catalysts for many enantioselective reactions such as enantiomeric epoxidation of unfunctionalized olefins, hydroxylations, oxidations, epoxidations, aziridinations,

CONTACT Dipali Sadhukhan dipali_juchem@yahoo.co.in Department of Chemistry, Indian Institute of Technology, Kharagpur, West Midnapur, West Bengal, India; Susanta Ghanta susanta.ghanta82@gmail.com Department of Chemistry, Indian Institute of Technology, Kharagpur, West Midnapur, West Bengal 721302, India.

Supplemental data for this article can be accessed at the publisher's website.

^c Preset address - Department of Chemistry, National Institute of Technology, Agartala, Tripura, India

© 2020 Taylor & Francis Group, LLC

cyclopropanation, Diels–Alder cyclization, kinetic resolution of racemic allenes, etc.^[3]

Use of chiral metal catalysts for the kinetic resolution of racemic secondary alcohols is a very important synthetic process as the enantiopure alcohols are the potential intermediates for several natural products, chiral ligands and biologically active compounds.^[4] Enantiomerically pure secondary alcohols are usually synthesized by the enzymatic kinetic resolution of secondary alcohols through acylation/deacylation,^[5] non-enzymatic kinetic resolution,^[6] and enantioselective reductions of ketones.^[7] Among the various kinetic resolution techniques, the most privileged method is the oxidative kinetic resolution (OKR) as molecular oxygen is used as the sole stoichiometric oxidant and water is formed as the only by-product. Although a number of chiral metal complexes of Ru,^[8] Pd,^[9] Mn,^[10] V^[11] and Ir^[12] have been used for the OKR of racemic secondary alcohols, those are expensive catalysts. Copper being a cheaper and more abundant metal, chiral Cu(II) complexes^[13] can be economically competent catalysts, although not very widely explored. In the present report, we have investigated the catalytic role of some chiral Schiff base-Cu complexes in the aforementioned oxidative kinetic resolution of racemic benzoin and to investigate the extent of chiral induction.

Herein we have synthesized chiral Schiff base ligands by the condensation of enantiopure amino alcohols (L-phenyl alaninol and L-valinol) and an aldehyde *o*-vanillin (2-hydroxy-3-methoxybenzaldehyde). The ligands were used to synthesize Cu(II) complexes that retain the chirality of the ligand. The ligands and the complexes were characterized by FT-IR and UV–Visible and circular dichroism spectroscopy. The structures of the complexes were established by single crystal X-ray diffraction. Analysis of the catalytic efficiency of the complexes for kinetic resolution of racemic benzoin has been investigated. To obtain a deeper understanding of the optical and chiroptical properties of molecules, density functional theory (DFT) and time dependent density functional theory (TD-DFT) calculations are necessary^[14] as those methods are reliable tools for the assignment and interpretation of electronic transitions involved in the optical properties. Hence in the present work, the structures of the ligands were optimized at the level of DFT in the relevant solvent phase. Time dependent density functional theory (TD-DFT) calculations complemented with quantum mechanics/molecular mechanics (QM/MM) studies have also been performed for the ligands and the complexes to understand the origins of the absorption and circular dichroism spectra.

Material and methods (experimental and theoretical)

Material

All solvents were of reagent grade and used after distillation. L-phenyl alanine, L-valine, sodium borohydride, iodine, potassium hydroxide, sodium sulfate, *o*-vanillin, sodium azide, benzoin and TEMPO were purchased from local chemical suppliers and used as received. Copper perchlorate

hexahydrate was prepared by treatment of copper carbonate (E.Merck, India) with 60% perchloric acid (E.Merck, India) followed by the slow evaporation on the steam bath. It was then filtered through a fine glass-frit and preserved in a CaCl₂ desiccator for further use.

Caution! Perchlorate salts are potentially explosive and should be used in less quantity and with much care although no such problem was encountered during the present experiments.

Physical measurements

The FT-IR spectra of the compounds were recorded on a Perkin Elmer RX I FT-IR spectrometer with KBr pellets in the range 4000–400 cm^{−1}. The electronic spectra were recorded at 300 K on a Shimadzu UV 2450 UV–Vis spectrometer using reagent grade methanol as solvent in the range 800–200 nm. ¹H and ¹³C-NMR spectra of the Schiff base ligands, benzoin and benzil were recorded on Bruker 400 MHz FT-NMR spectrometer using tetramethylsilane as internal standard in CDCl₃ solvent. The CD spectra of the samples were recorded with a Jasco J 815 CD spectrometer.

Crystallographic data collection and structure refinements

The X-ray diffraction data were collected on a Bruker Apex II Kappa CCD diffractometer containing area detector and graphite monochromator with MoK α radiation ($\lambda = 0.71069$ Å) at 293 K. Data collection and data reduction were performed with SHELX^[15] programmes. The structures were solved by direct method using the program SIR92^[16] and refined with the program CRYSTALS.^[17] All non-hydrogen atoms were refined anisotropically by full-matrix least-squares based on *F*. All other H atoms were generated geometrically and were included in the refinement in the riding model approximation. The crystallographic data for the complexes are summarized in Table S8.

Theoretical calculations

The DFT and TD-DFT calculations have been performed using the Gaussian 09 program package.^[18] The structures of the ligands were optimized at the B3LYP level of theory.^[19] The various vertical Franck–Condon electronic transitions were calculated at the TD-DFT level of theory using 6-31 g* basis set.^[20] The optimization calculations have been done by applying the self-consistent reaction field (SCRF) under the polarizable continuum model (c-pcm) including methanol as the solvent.^[21] We have considered first fifty excitations for TD-DFT calculation for both ligands and complex molecules. The ground state optimized structures were considered for all excited state calculations for the ligands (L¹H₂ and L²H₂) while for the complexes (C1 and C2), the initial structures were taken from the X-ray diffraction CIF files. CAM-B3LYP method is employed for TD-DFT calculation for both complexes.

Syntheses of the ligands and the complexes

Synthesis of the ligands: 2-(3-benzyl-4-hydroxybut-1-enyl)-6-methoxyphenol (L^1H_2) and 2-(4-hydroxy-3-isopropylbut-1-enyl)-6-methoxyphenol (L^2H_2)

The ligands L^1H_2 and L^2H_2 were synthesized in two steps following the procedure depicted in Scheme 2.

In the first step, L-phenyl alanine (for L^1H_2)/L-valine (for L^2H_2) were reduced to L-phenyl alaninol/L-valinol according to the published procedure.^[22] In the second step, L-phenyl alaninol (10 mmol, 1.51 g)/L-valinol (10 mmol, 1.03 g) were mixed with o-vanillin (10 mmol, 1.52 g) in 50 mL methanol and the mixture was refluxed at 65 °C for 6 h. Yellow solutions of L^1H_2 and L^2H_2 were obtained. The L^1H_2 solution on vacuum evaporation resulted in a yellow powder which was recrystallized from methanol. Yellow crystals of the ligand L^1H_2 were obtained by slow evaporation of the methanolic solution in 2 days. L^2H_2 was obtained as a viscous oily liquid.

L^1H_2 : Yield: 185 mg (65%). 1H -NMR (ppm, 400 MHz, $CDCl_3$) 8.08 (1H, s, H_7), 7.262–7.228 (3H, m, H_{14-16}), 7.190–7.138 (3H, m, H_{4-6}), 6.896–6.751 (2H, m, $H_{13,17}$), 3.928 (3H, s, H_{1-3}), 3.903–3.753 (2H, m, $H_{9,10}$), 3.538–3.487 (1H, m, H_8), 3.016–2.982 (1H, m, H_{11}), 2.896–2.841 (1H, m, H_{12}) (Figure S5). ^{13}C -NMR (ppm, 100 MHz, $CDCl_3$) δ 166.2 (C_8), 152.1 (C_2), 148.6 (C_7), 137.8 (C_{12}), 129.6 ($C_{14, 16}$), 128.6 ($C_{13, 17}$), 126.6 (C_6), 123.3 (C_{15}), 118.3 (C_3), 118.1 (C_5), 114.2 (C_4), 72.9 (C_{10}), 66.0 (C_9), 56.2 (C_1), 39.2 (C_{11}) (Figure S6) (Scheme 3a). FT-IR (KBr, cm^{-1}): 3439w, 3220w, 2928w, 2854w, 1638s, 1508m, 1497m, 1458m, 1248s, 1216s, 1162m, 1090s, 1050m, 1013w, 965w, 911w, 848w, 789w, 752m, 718m, 702m, 605w, 558w, 467w. UV-Vis (MeOH) λ_{max} nm (ϵ Lmol $^{-1}cm^{-1}$): 330 (2900), 262 (14,400), 220 (69,200).

L^2H_2 : Yield: 243 mg (89%). 1H -NMR (400 MHz, $CDCl_3$, ppm): 8.33 (1H, s, H_7), 6.97–6.87 (2H, m, $H_{4,6}$), 6.79–6.76 (1H, m, H_5), 3.9 (3H, s, H_{1-3}), 3.89–3.82 (2H, m, $H_{9,10}$), 3.78–3.73 (1H, m, H_8), 1.98–1.93 (1H, m, H_{11}), 0.95 (6H, d, J = 8 Hz, H_{12-17}) (Figure S7). ^{13}C -NMR (ppm, 100 MHz, $CDCl_3$) δ 166.0 (C_8), 152.9 (C_2), 148.8 (C_7), 123.2 (C_6), 118.3 (C_5), 117.9 (C_4), 114.0 (C_3), 64.6 (C_{10}), 56.2 (C_1), 30.1 (C_9), 19.9 (C_{11}), 18.4 ($C_{12, 13}$) (Figure S8) (Scheme 3b). FT-IR (MeOH, cm^{-1}): 3629–3020w, 2942–2847w, 1630s, 1465s, 1390s, 1404s, 1248s, 1176–1142m, 1083m, 1022m, 961m, 896m, 840m, 770m, 720s, 657m, 614m, 544m. UV-Vis (MeOH) λ_{max} nm (ϵ Lmol $^{-1}cm^{-1}$): 418 (9600), 245–294 (43,000–25,700), 222 (79,800).

Synthesis of the complex $[Cu_4(L^1H)_2(L^1)_2](ClO_4)_2$ (C1)

$Cu(ClO_4)_2 \cdot x H_2O$ (0.5 mmol, 0.187 g) was dissolved in 15 mL methanol. Solid L^1H_2 (0.5 mmol, 0.142 g) was added into it while stirring at room temperature ($\sim 35^\circ C$). Aqueous solution of NaN_3 (1.5 mmol, 0.09 g) was added drop wise into the reaction mixture. The solution was stirred for $\frac{1}{2}$ h. The green solution was filtered and kept for slow evaporation at room temperature. On the next day, green prismatic single crystals appeared. Yield 166 mg (82%). Anal. Calc. for $[C_{68}H_{74}Cl_2Cu_4N_4O_{22}]$: C, 50.28; H,

4.59; N, 3.45. Found: C, 50.24; H, 4.56; N, 3.49. FT-IR (KBr) ν cm^{-1} : 3054w, 3024w, 2934w, 2830w, 1635s, 1601s, 1557m, 1539m, 1520w, 1506w, 1489w, 1467s, 1454s, 1446s, 1373w, 1360w, 1322w, 1295w, 1250s, 1220s, 1084s, 1048w, 973m, 853w, 776w, 737m, 703m, 652w, 624m, 586w, 503w, 470w, 454w, 443w. UV-Vis (MeOH) λ_{max} nm (ϵ Lmol $^{-1}cm^{-1}$): 681(d-d transition), 378 (15,400), 281 (51,400), 236 (88,300), 209 (84,000).

Synthesis of the complex $[Cu_4(L^2)_4Na_2(DMF)_2(H_2O)](ClO_4)_2$ (C2)

$Cu(ClO_4)_2 \cdot x H_2O$ (0.5 mmol, 0.187 g) was dissolved in 10 mL methanol. Methanolic solution of L^2H_2 (0.5 mmol, 10 mL) was added into it while stirring at room temperature ($\sim 30^\circ C$). Aqueous solution of NaN_3 (1.5 mmol, 0.09 g) was added drop wise into the reaction mixture. The solution was stirred for $\frac{1}{2}$ h. The green solution was filtered and kept for slow evaporation at room temperature. Green solid precipitated upon evaporation for 1 week. The precipitate was dissolved in 20 mL 1:1 DMF-MeOH mixture and the solution was settled for slow evaporation at RT. Green block shaped crystals appeared after three weeks. Yield 126 mg (63%). Anal. Calc. for $[C_{58}H_{84}Cl_2Cu_4N_6Na_2O_{23}]$: C, 43.42; H, 5.28; N, 5.24. Found: C, 43.45; H, 5.26; N, 5.26. FT-IR (KBr) ν cm^{-1} : 3650–3100w, 2960m, 2872m, 1640s, 1587m, 1554m, 1468s, 1447s, 1430m, 1404m, 1326s, 1256s, 1219s, 1170m, 1082s, 1052s, 979m, 882m, 735s, 666m, 587m, 518m. UV-Vis (MeOH) λ_{max} nm (ϵ Lmol $^{-1}cm^{-1}$): 685 (d-d transition), 378 (15,400), 277 (55,700), 233 (100,600), 207 (94,700).

General procedure for AOKR

The catalyst was dissolved in 10 mL solvent. TEMPO was added in it and stirred for 5 min. Benzoin (1 mmol, 212 mg) was then added and the reaction was continued employing O_2 atmosphere (using O_2 balloon), varying temperature and reaction time. After completion, the reaction mixture was diluted with ethyl acetate and washed with dilute HCl followed by H_2O . The organic layer was dried over anhydrous Na_2SO_4 , concentrated under vacuum, and the resulting residue was purified by silica gel column chromatography (hexane:ethylacetate 20:1) to separate the benzil and the unreacted benzoin successively. The enantiomeric excess (%) of recovered benzoin was determined by HPLC using a Daicel ChiralPAK AS-H column (MeOH, 1 mL/min, 254 nm): t_R (major, 12.303 min), t_R (minor, 13.118 min).

Benzoin: 1H -NMR (ppm, 400 MHz, $CDCl_3$) δ 7.84–7.82 (2H, m), δ 7.46–7.42 (1H, m), δ 7.34–7.30 (2H, m), δ 7.27–7.18 (4H, m), δ 5.88–5.86 (1H, d, J = 6 Hz), δ 4.47–4.46 (1H, d, J = 6 Hz) (Figure S9). ^{13}C -NMR (ppm, 100 MHz, $CDCl_3$) δ 194.8, 129.8, 125.0, 124.6, 124.5, 123.7, 72.1 (Figure S10).

Benzil: 1H -NMR (ppm, 400 MHz, $CDCl_3$) δ 7.99–7.97 (4H, m), δ 7.68–7.64 (2H, m), δ 7.54–7.50 (4H, m) (Figure S11). ^{13}C -NMR (ppm, 100 MHz, $CDCl_3$) δ 190.5, 130.8, 128.9, 125.8, 124.9 (Figure S12).

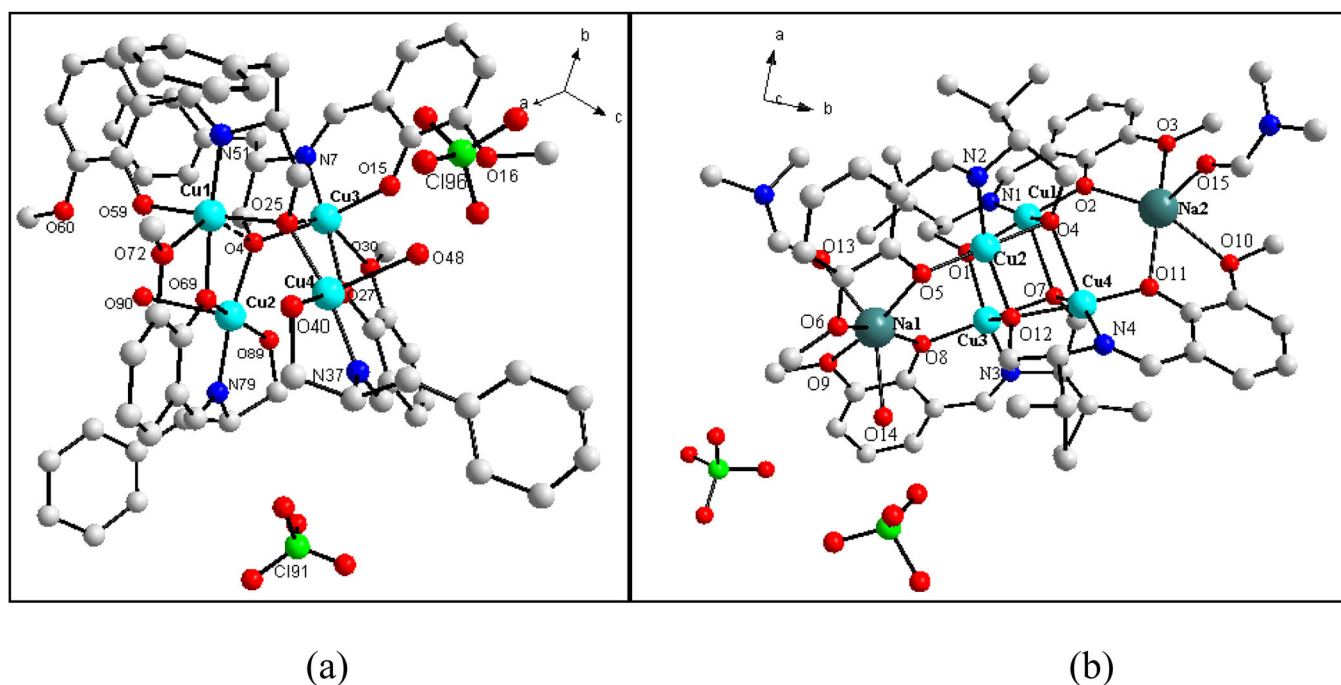


Figure 1. The asymmetric unit of **C1** (a) and **C2** (b). Hydrogen atoms are omitted for clarity.

Results and discussions

Crystal structure of $[\text{Cu}_4(\text{L}^1\text{H})_2(\text{L}^1)_2](\text{ClO}_4)_2$ (**C1**) and $[\text{Cu}_4(\text{L}^2)_4\text{Na}_2(\text{DMF})_2(\text{H}_2\text{O})](\text{ClO}_4)_2$ (**C2**)

The asymmetric unit of the complexes **C1** and **C2** are illustrated in Figure 1a,b, respectively. Selected bond lengths and angles of **C1** are listed in Tables S1 and S2, respectively, and that of **C2** are listed in Tables S3 and S4, respectively.

The asymmetric unit of both complexes consists of a Cu_4O_4 core where four copper atoms are bridged by two μ_3 -hydroxo (O4, O25) and two μ -phenoxo oxygens (O27, O69) in **C1** but by four μ_3 -hydroxo oxygens (O1, O4, O7 and O12) in **C2** in an approximately cubic array of alternate copper and oxygen atoms occupying the vertices of a cube. In **C1**, among the twelve edges, two connecting Cu2–O27 and Cu4–O69 are missing and Cu2 and Cu4 being at the open corners maintain a large distance from each other ($\text{Cu2}\cdots\text{Cu4} \approx 3.8 \text{ \AA}$) while the oxygen bridged Cu \cdots Cu distances are within 3.2–3.4 \AA . Hence, the tetranuclear unit forms an open or pseudo-cubane structure of Cu_4O_4 core (Figure 2a) whereas complex **C2** features a full cubane of 4 + 2 type^[23] with four short distances of approximately 3.1 \AA between Cu1 \cdots Cu2, Cu1 \cdots Cu3, Cu2 \cdots Cu4, Cu3 \cdots Cu4 and 2 long distances of approximately 3.3 \AA between Cu1 \cdots Cu4, Cu2 \cdots Cu3 (Figure 2b).

In **C1**, two of the phenoxo oxygens (O4 and O25) being involved in Cu–Cu bridging, have lost the potential to coordinate to any other metal ion outside the pseudo-cubane core whereas in **C2**, the phenoxo oxygens (O2, O5, O8 and O11) being exempted from building the cubane core, gets involved in the formation of outer compartments along with methoxo oxygens (O3, O6, O9 and O10) where two Na^+ ions are accommodated.

Each Cu(II) ion lies in a penta coordinated NO_4 square pyramidal environment in both complexes. The Addison parameter^[24] $\tau = 0.00, 0.11, 0.04$ and 0.08 for Cu1–Cu4, respectively,

in **C1** indicates very small distortion from ideal SP geometry but the SP environment is more distorted in **C2** as evident from the τ values 0.29, 0.27, 0.31 and 0.37 for Cu1–Cu4, respectively. In **C1**, the basal plane around Cu1 and Cu3 is formed by the imine nitrogen, phenoxo oxygen, μ_3 -hydroxo oxygen from one ligand $(\text{L}^1)^{2-}$ and μ -phenoxo oxygen from a second interconnecting ligand $(\text{HL}^1)^-$, the methoxo oxygens from the respective interconnecting ligands occupy the apical positions. The square pyramids around Cu2 and Cu4 are formed by equatorially coordinated imine nitrogen, hydroxo oxygen, μ -phenoxo oxygen from one ligand $(\text{HL}^1)^-$ and μ_3 -hydroxo oxygen from another ligand $(\text{L}^1)^{2-}$ and apical water molecule. The basal Cu–O/N bond lengths are within the range of 1.88–2.08 \AA whereas the apical Cu–O bonds are more elongated (2.25–2.45 \AA) owing to Jahn–Teller effect. If the hydroxo oxygens O4 and O25 are considered to be μ_3 -bridging and the elongated Cu1–O4 and Cu3–O25 bonds are taken into account, the polyhedra around Cu1 and Cu3 turn to be a highly distorted octahedra (or pseudo octahedra) as the *trans* angles between the axial ligands ($\angle \text{O4–Cu1–O72} = 143.48^\circ$ and $\angle \text{O25–Cu3–O30} = 143.42^\circ$) are highly deviated from the ideal value (180°). In **C2**, the square pyramid around each Cu is formed by imine nitrogen, μ -phenoxo oxygen and three μ_3 -hydroxo oxygens from three different ligands. The apical Cu–(μ_3)O distance (2.25–2.35 \AA) is longer than the two basal Cu–(μ_3)O components (1.88–1.99 \AA) indicating Jahn–Teller distortion. All these bond lengths are in good agreement with those previously reported in the literature.^[25] The Na^+ ions in the outer sphere of **C2** are equatorially coordinated by μ -phenoxo and methoxo oxygens from two adjacent ligands. One DMF and one H_2O complete the octahedral coordination sphere of Na1 whereas one apical position of Na2 is coordinated by a DMF molecule resulting in a highly distorted SP geometry ($\tau = 0.39$). The equatorial coordination plane around Na1 is almost perpendicularly oriented with respect to that of Na2.

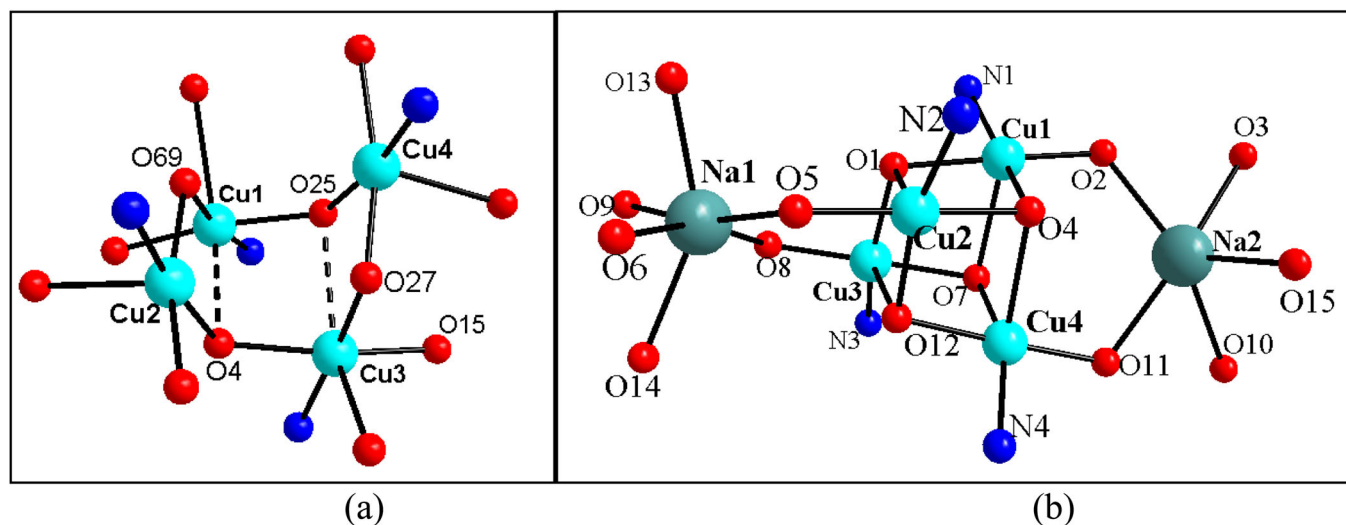


Figure 2. Structural representation of the Cu₄O₄ pseudo cubane core of C1 (a) and cubane core of C2 (b).

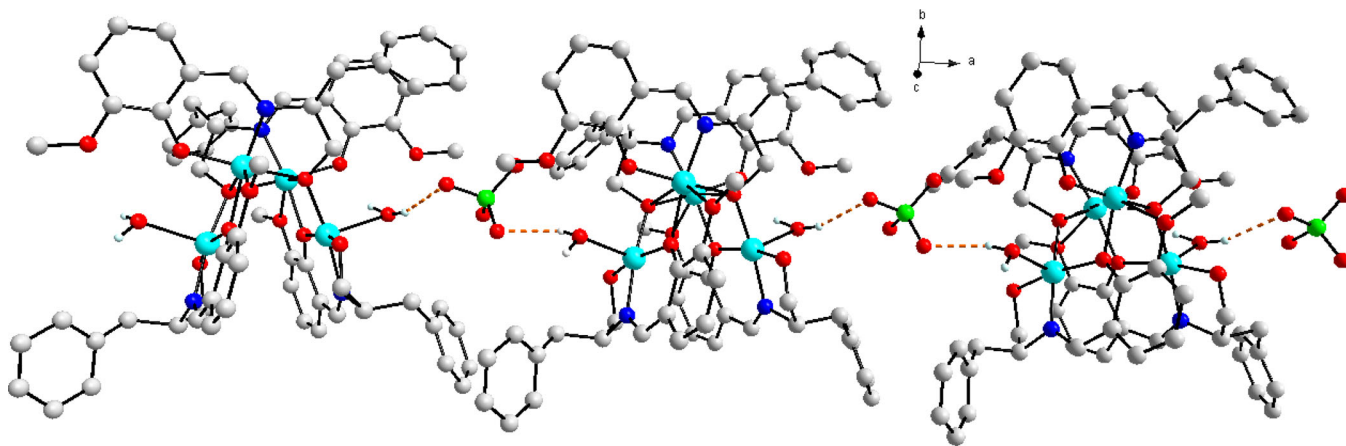


Figure 3. The hydrogen bonding features in C1. Hydrogen atoms and perchlorate molecules not involved in hydrogen bonding are omitted for clarity.

The tetranuclear [Cu₄(L¹H)₂(L¹)₂] unit of C1 is dicationic as two of the ligands are monobasic and two ClO₄[−] ions are present in the lattice to counterbalance the charge of the complex. One of the perchlorate ions interconnects the coordinated H₂O ligands of adjacent tetranuclear units through hydrogen bonds: O48–H482...O98 and O90–H902...O97 (Table S5).

Thus, an infinite one dimensional supramolecular chain is formed by interconnected tetranuclear cationic complex units mediated by ClO₄[−] ions (Figure 3).

Fourier transform infrared spectroscopy

The IR spectra of the complexes (C1 and C2) were analyzed in comparison with that of the respective free ligands L¹H₂ and L²H₂ in 4000–400 cm^{−1} region (Figures S1–S4). The ligands showed broad O–H stretching bands around 3229 (L¹H₂) and 3240 (L²H₂) cm^{−1} and C–H stretching bands around 2945 (L¹H₂) and 2930 (L²H₂) cm^{−1}. In the spectrum of the free ligand, imine stretching bands appeared at 1638 (L¹H₂) and 1630 (L²H₂) cm^{−1}, but in the respective complexes the characteristic imine bands were observed slightly shifted 1635 (C1) and 1640 (C2) cm^{−1} indicating the

coordination of the imine nitrogen atom to the metal center.^[26,27] The characteristic stretching band for perchlorate anion appeared in the region 1084 and 1082 cm^{−1}, respectively, for C1 and C2. Ligand coordination to the metal center is substantiated by weak bands appearing at 454 and 443 cm^{−1} in C1 which are mainly attributed to Cu–N stretching bands in the complex. The Cu–N stretching bands in C2 and the Cu–O stretching bands in C1 and C2 are beyond the limit of the instrument.

UV-Visible spectroscopy

The electronic spectra of the ligands and the complexes (Figure 4) were analyzed in MeOH solution (10^{−5} M) in the region 200–800 nm. The spectrum of the free L¹H₂ ligand shows several $\pi \rightarrow \pi^*$ transitions at λ_{max} 330, 262 and 220 nm. In case of free L²H₂ several $\pi \rightarrow \pi^*$ transitions appear at 294–245 and 222 nm. An $n \rightarrow \pi^*$ transition band is observed at 418 nm in L²H₂ which is not prominent in L¹H₂; possibly overwhelmed by the $\pi \rightarrow \pi^*$ transitions, as L¹H₂ contains greater number of conjugated π systems than L²H₂. In the spectrum of both the complexes (C1 and C2) LMCT band

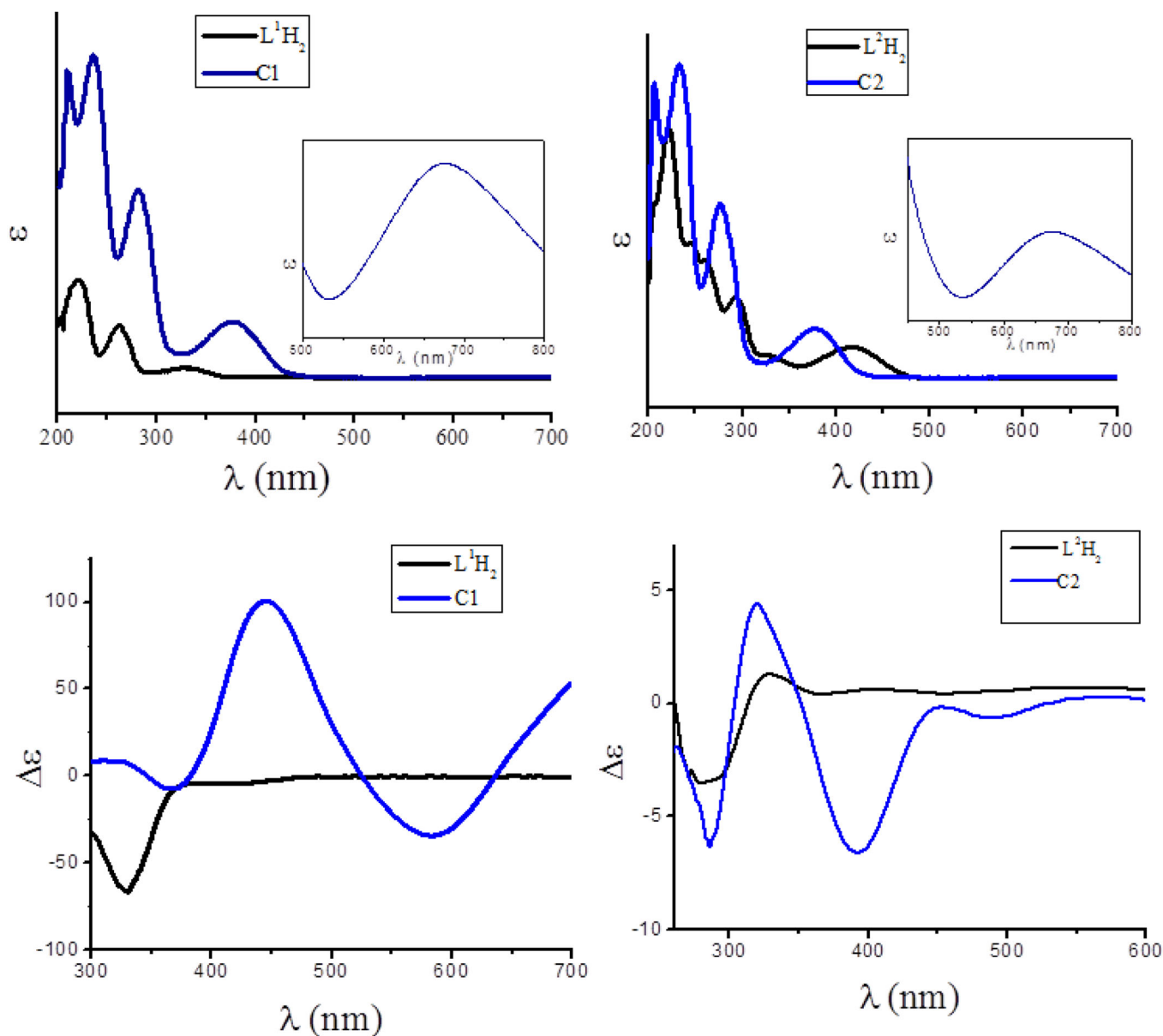


Figure 4. UV-Visible spectra (MeOH, 10^{-5} M) and CD spectra (MeOH, 10^{-3} M) of the ligands (black line) and the complexes (blue line). The d→d transition bands of **C1** and **C2** are presented as inset.

appears at 378 nm. $\pi \rightarrow \pi^*$ transition bands are red shifted to 281 and 236 nm in **C1** and to 277 and 233 nm in **C2**.

A high energy CT band appears in the absorption spectrum of the complexes upon coordination of the ligands to metal center. Hence the sharp peaks at 207 nm in both the complexes can be attributed to ligand→ligand charge transfer transition (LLCT).^[28] The d→d transition bands of much weaker intensity appear around 681 nm in **C1** and 685 nm in **C2** and are characteristics of square pyramidal Cu (II) metal ion (inset in Figure 4).^[29]

Circular dichroism

The circular dichroism spectra of the ligands and the complexes have close resemblance with their respective absorption spectra (Figure 4). In methanolic solution (10^{-3} M) **L¹H₂** shows a distinct negative signal at 330 nm that

corresponds to the $n \rightarrow \pi^*$ transition of its absorption spectrum. **L²H₂** shows a negative CD signal at 280 nm corresponding to $\pi \rightarrow \pi^*$ transition. Complex **C1** exhibits two negative signals at 365 and 584 nm that correspond to the LMCT and d→d transitions, respectively. **C2** exhibits LMCT and d→d transition bands at 390 nm and 490 nm, respectively, along with a $\pi \rightarrow \pi^*$ transition signal at 280 nm.

Computational analysis

In order to understand the transitions involved in the UV-Visible and circular dichroism spectra of the ligands and the complexes, DFT and TD-DFT were calculated.^[30] The simulated spectral transitions along with the experimental transitions are listed in Table S6.

The calculated UV-Visible and CD spectra of the ligands are displayed in Figure 5.

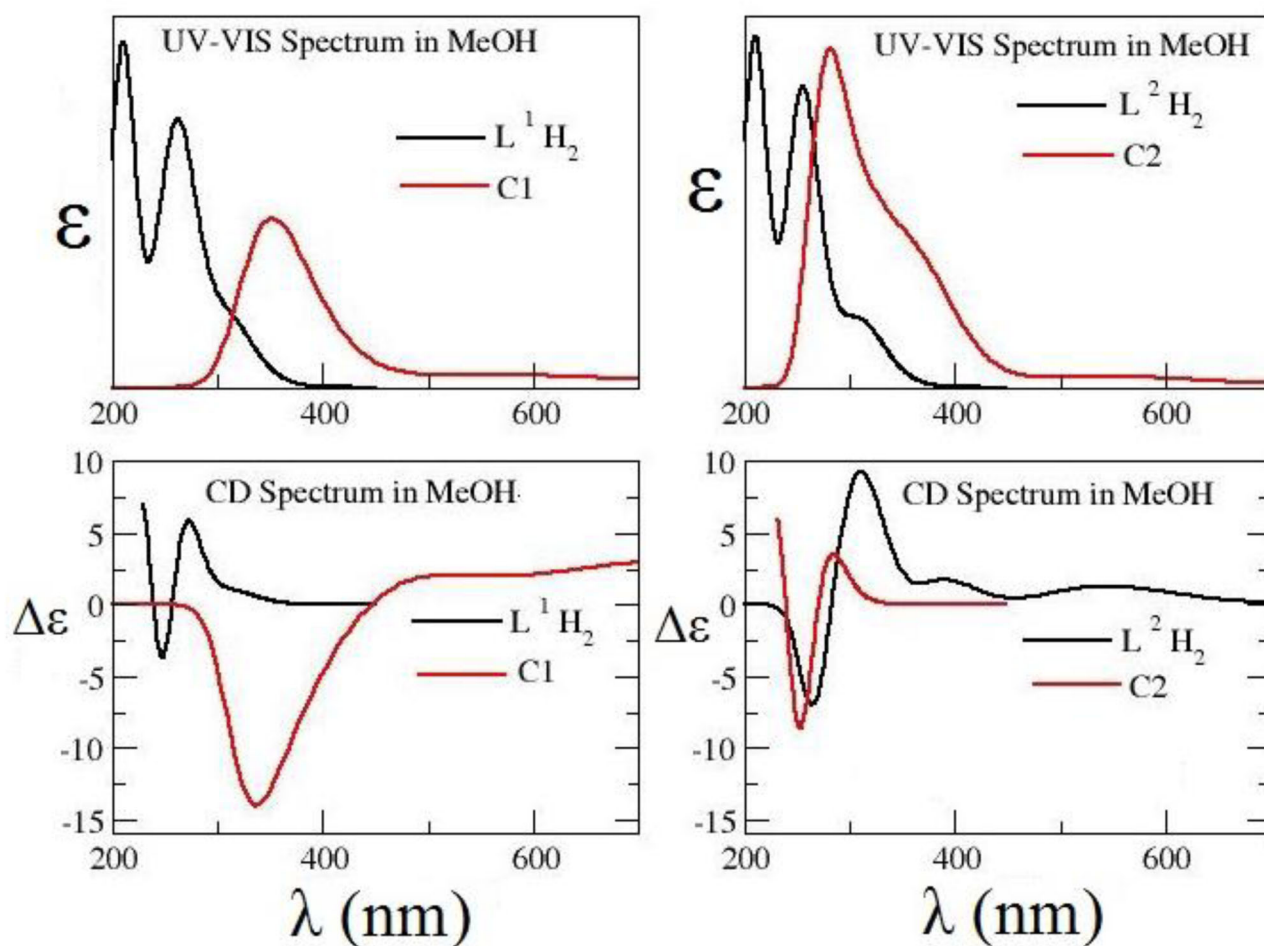


Figure 5. The TD-CAM-B3LYP calculated UV-Visible and CD spectra of the ligands (black line) and the complexes (red line).

A good overall agreement has been found between the experimental and the simulated spectra. The B3LYP computed HOMO and LUMO frontier molecular orbitals (FMOs) of both L^1H_2 and L^2H_2 are shown in Figure 6 which explains the origin of transitions. For L^1H_2 the $\pi \rightarrow \pi^*$ transitions were calculated around 312, 266 and 213 nm attributed to HOMO to LUMO, HOMO-1 to LUMO and HOMO to LUMO + 3 excitations, respectively.

The computed absorption bands in L^2H_2 appear around 310, 256 and 213 nm due to $\pi \rightarrow \pi^*$ transitions from HOMO to LUMO, HOMO-1 to LUMO and HOMO to LUMO + 1, respectively. The simulated CD spectra for both ligands show a negative signal around 250 nm. The qualitative features of the simulated CD spectra are in good agreement with the experimental spectra, the blue shift of the band positions can be attributed to approximations in both the density functional and treatment of solvent effect.^[31] For TD-DFT calculation of the complexes we ignored the anions and considered the bipoisitive complex cations only, hence an overall spin multiplicity five has been taken into account. For **C1** a very intense absorption band appeared at 355 nm accompanied by a much weaker band around 586 nm (Figure 5). The lowest energy band is an overlap of ligand to metal charge transfer (LMCT) and d→d transitions whereas the intense band at 355 nm is due to the ligand to

ligand charge transfer (LLCT). The MO diagram for the LMCT transition of **C1** is shown in Figure 7.

In the simulated absorption spectrum of **C2** (Figure 5), three peaks are observed, the most intense peak is centered at 280 nm, a shoulder is observed around 374 nm and a very weak peak appears around 554 nm. The lowest energy excitation is for the d to d transition of Cu metal as observed in the corresponding MO diagram shown in Figure 7. The other two excitations are due to ligands $\pi \rightarrow \pi^*$ transitions. In the simulated CD spectra of both the complexes a distinct negative signal appears around 250 nm.

Oxidative kinetic resolution of racemic benzoin

Enantiopure benzoin is usually synthesized by (i) enzymatic hydrolysis such as benzaldehyde lyase (BAL) or benzoylformate decarboxylase (BFD) enzyme,^[32] (ii) multistep enantioselective benzoin condensations by using polycyclic triazolium salt or its analogues as catalysts.^[33] Our effort is to synthesize enantioenriched benzoin by a single step and non-enzymatic process. In this article, we report our initial findings regarding chiral Schiff base-Cu(II) complex catalyzed oxidative kinetic resolution of racemic benzoin. (±) Benzoin was reacted with 2,2,6,6-tetramethylpiperidin-1-oxyl (TEMPO) and the enantiopure chiral complexes **C1** and **C2**

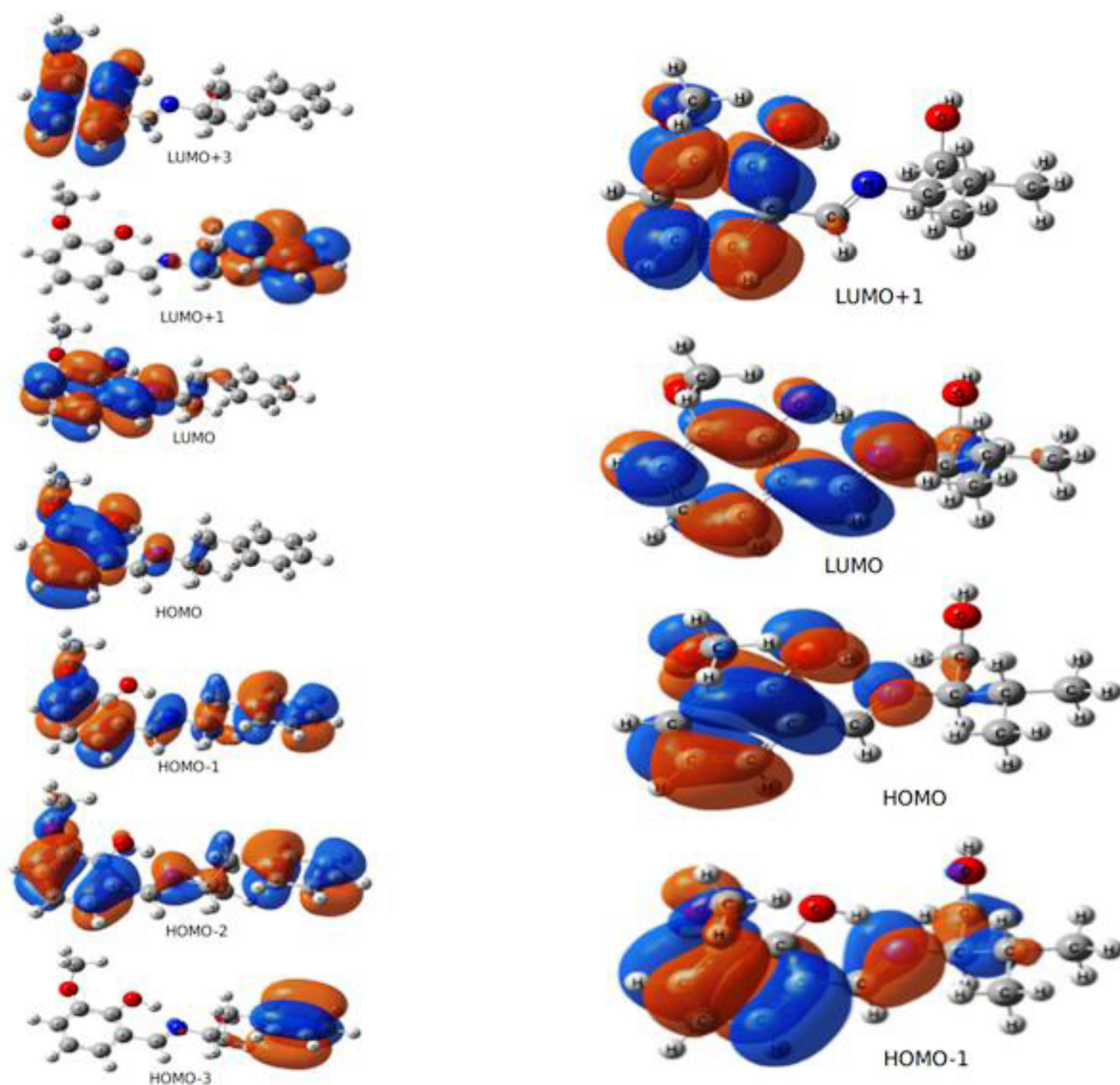


Figure 6. Calculated highest occupied and lowest unoccupied molecular orbitals of L^1H_2 (left) and of L^2H_2 (right).

in the presence of molecular oxygen. The oxidized product benzil is obtained and the unreacted benzoin was recovered in enantiomerically enriched form (Scheme 1). To optimize the reaction conditions we have varied the percentage of TEMPO and the catalysts, solvent, temperature and reaction time as listed in Table S7.

We have performed solvent screening based on the solubility of the catalysts (**C1** and **C2**). Acetonitrile is found to be the most suitable solvent in terms of ready solubility of the catalysts as well as enantioselectivity. Oxidation of benzoin not at all occurs at room temperature even after prolonged reaction time. Conversion and selectivity increase upon refluxing the reaction mixtures in the respective solvents. No oxidation product was detected without TEMPO. When the oxidation was carried out only with TEMPO and without the catalysts a trace amount of oxidized product

benzil was detected and the unreacted benzoin was recovered almost quantitatively which suggests that no side reaction is taking place due to TEMPO. The S(+) enantiomer of racemic benzoin was oxidized faster to the corresponding benzil and the slower-reacting R(-) enantiomer was recovered in enantiomerically enriched form (Figures S13–S15). The configuration of the recovered benzoin was determined by comparing the optical rotation value with the literature value.^[13] The reaction conditions, as mentioned in entry 17 were found to be the optimum for a moderate (63%) enantiomeric excess using **C1** as the catalyst. At similar conditions using **C2** as the catalyst we obtained 45% excess of the R(-) enantiomer of benzoin. From the previously reported mechanism of oxidative kinetic resolution of secondary alcohols^[34] it can be anticipated that the substrate and the oxidant bind to the metal center in intermediate

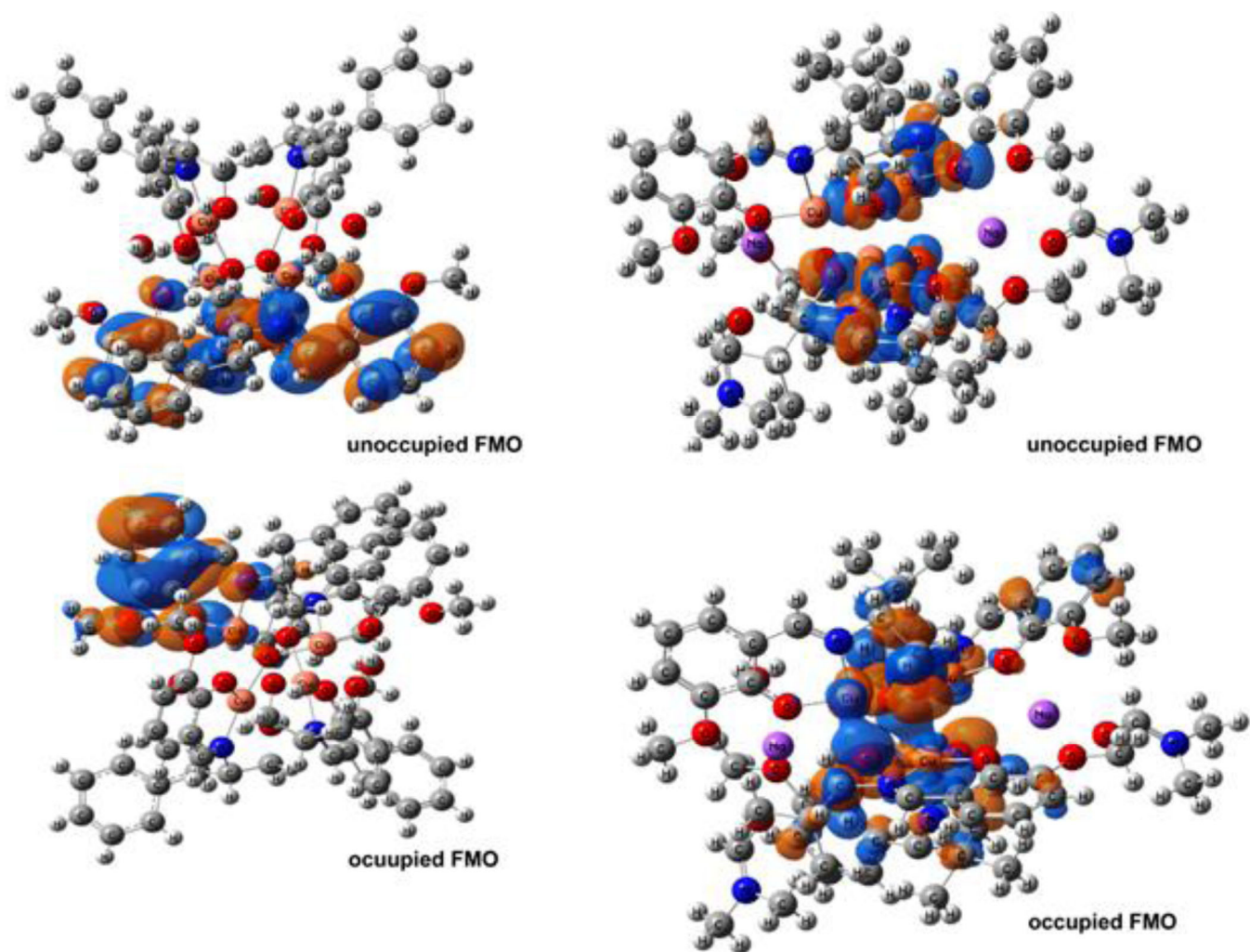
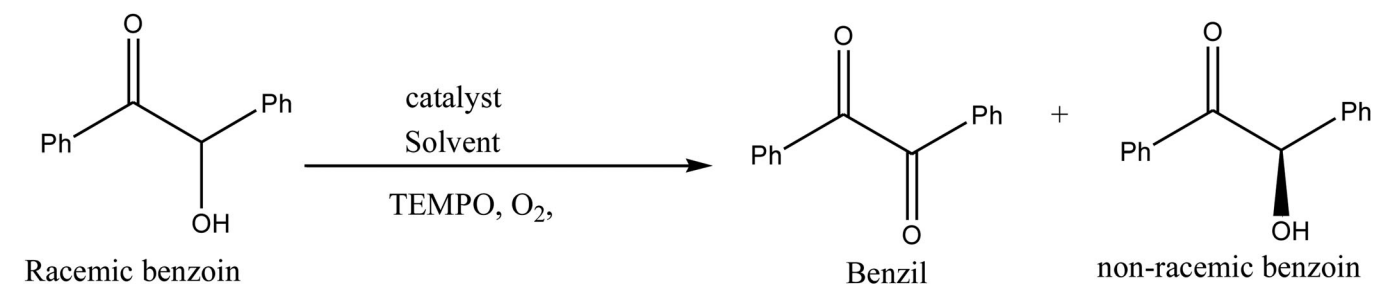
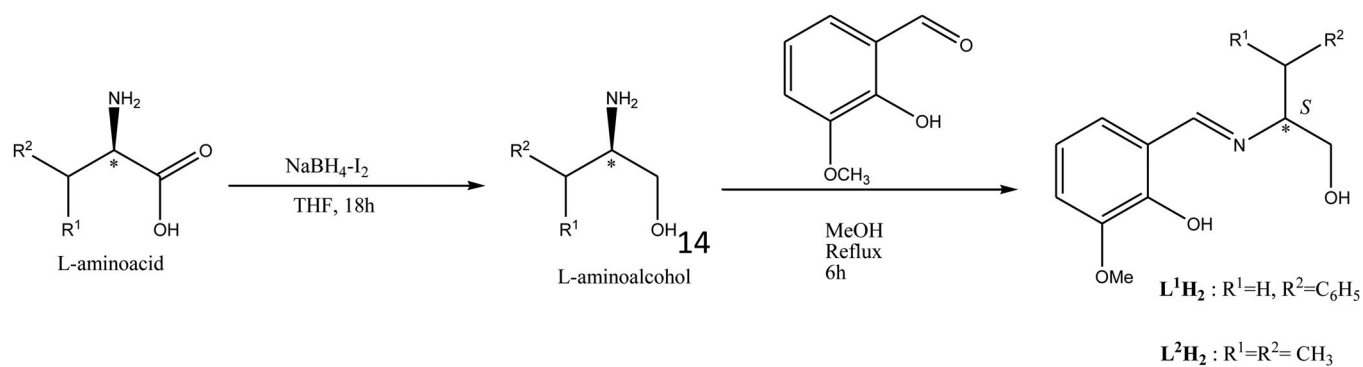


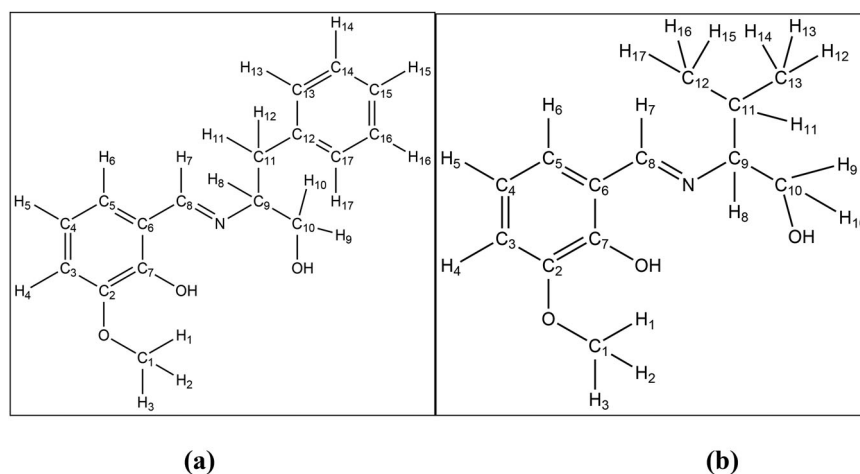
Figure 7. The Frontier molecular orbitals for the LMCT transition in C1 (left) and in C2 (right).



Scheme 1. Oxidative kinetic resolution of (±) benzoin



Scheme 2. Synthetic route of the Schiff base ligands



Scheme 3. The proton and carbon numbering scheme of (a) L^1H_2 and (b) L^2H_2

steps. All Cu^{II} centers in **C1** and **C2** are penta-coordinated. Hence, they have one vacant coordination site to bind with the substrate (benzoin) and oxygen. Moreover, in both complexes, the oxo-bridged Cu-Cu distance lies between 3.1 and 3.4 Å which is favorable for substrate-oxygen interaction. Now, in **C1** the Cu_4O_4 cubane core is open (Figure 2), hence, both benzoin and oxygen can easily approach the Cu center to bind with. Moreover, Cu2 and Cu4 have labile H_2O ligand at their axial coordination site which can leave during the reaction and provide two vacant sites for both substrate and oxygen to coordinate at the same metal center and the reaction is highly favored. In case of **C2**, the cubane core is closed (Figure 2); hence the Cu centers are difficult for the reactants to approach. The bulky Na ions also disfavor this process. Thus, the lower efficacy of **C2** compared to **C1** is justified from the structural point of view.

Conclusion

We have successfully synthesized two tetranuclear $Cu(II)$ complexes with interesting variations in the cubane like core structures. The absorption and circular dichroism spectral features of the ligands and the complexes are in good agreement with that calculated through TD-DFT. Ligand induced chirality is present in the complexes as evident from the experimental and calculated circular dichroism spectroscopy. The complexes have been examined as catalysts for the enantioselective oxidative kinetic resolution of racemic benzoin. A maximum of 63% enantio-enriched benzoin has been isolated using **C1** as catalyst. The catalytic activities of the complexes are well correlated to their structural features.


Acknowledgments

SG thanks IIT Kharagpur and NIT Agartala for computational facilities. This work was supported by the Indian Institute of Technology, Kharagpur.

Conflict of interest

The authors have no conflict of interest.

ORCID

Dipali Sadhukhan  <https://orcid.org/0000-0001-8176-9222>
 Prithwi Ghosh  <https://orcid.org/0000-0001-5243-751X>
 Susanta Ghanta  <http://orcid.org/0000-0002-7095-5107>

References

- (a) Cao, W.; Feng, X.; Liu, X. *Org. Biomol. Chem.* **2020**, 9, 93–96. (b) Fache, F.; Schulz, E.; Tommasino, M. L.; Lemaire, M. *Chem. Rev.* **2000**, 100, 2159–2232. (c) Tokairin, Y.; Shigeno, Y.; Han, J.; Röscenthaler, G.-V.; Konno, H.; Moriawaki, H.; Soloshonok, V. A. *ChemistryOpen* **2020**, 9, 93–96.
- (a) Katsuki, T. In *Catalytic Asymmetric Synthesis*; Ojima, I., Ed.; Wiley: New York, **2000**; Chapter 6, p 287. (b) Jacobsen, E. N.; Wu, M. H. In *Comprehensive Asymmetric Catalysis II*; Jacobsen, E. N., Pfaltz, A., Yamamoto, H., Eds.; Springer-Verlag: New York, **1999**; Chapter 18, p 649. (c) Jacobsen, E. N.; Zhang, W.; Güler, M. L. *J. Am. Chem. Soc.* **1991**, 113, 6703–6704. (d) Jacobsen, E. N.; Zhang, W.; Muci, A. R.; Ecker, J. R.; Deng, L. *J. Am. Chem. Soc.* **1991**, 113, 7063–7064. (e) Zhang, W.; Jacobsen, E. N. *J. Org. Chem.* **1991**, 56, 2296–2298. (f) Palucki, M.; McCormick, G. J.; Jacobsen, E. N. *Tetrahedron Lett.* **1995**, 36, 5457–5460.
- (a) Smith, K.; Liu, C. *Chem. Commun.* **2002**, 886–887. DOI: [10.1039/B200246A](https://doi.org/10.1039/B200246A) (b) Canali, L.; Sherrington, D. C. *Chem. Soc. Rev.* **1999**, 28, 85–93. (c) Ito, Y. N.; Katsuki, T. *Bull. Chem. Soc. Jpn.* **1999**, 72, 603–619.
- (a) Pellissier, H. *Tetrahedron* **2018**, 74, 3459–3468. (b) Kunisu, T.; Oguma, T.; Katsuki, T.; *J. Am. Chem. Soc.* **2011**, 133, 12937–12939. (c) Jacobsen, E. N.; Pfaltz, A.; Yamamoto, H. *Comprehensive Asymmetric Catalysis*; Springer: Berlin, 1999; Vols. 1–3. DOI: [10.1016/j.tet.2018.05.015](https://doi.org/10.1016/j.tet.2018.05.015).
- Jammi, S.; Rout, L.; Saha, P.; Akkilagunta, V. K.; Sanyasi, S.; Punniyamurthy, T. *Inorg. Chem.* **2008**, 47, 5093–5098. DOI: [10.1021/ic800228c](https://doi.org/10.1021/ic800228c).
- (a) Sekar, G.; Nishiyama, H. *J. Am. Chem. Soc.* **2001**, 123, 3603–3604. DOI: [10.1021/ja010029i](https://doi.org/10.1021/ja010029i) (b) Sekar, G.; Nishiyama, H. *Chem. Commun.* **2001**, 1314–1315. DOI: [10.1039/B102460B](https://doi.org/10.1039/B102460B).
- Ager, J. D.; Laneman, A. S. *Tetrahedron: Asymmetry* **1997**, 8, 3327–3355. DOI: [10.1016/S0957-4166\(97\)00455-2](https://doi.org/10.1016/S0957-4166(97)00455-2).
- Masutani, K.; Uchida, T.; Irie, R.; Katsuki, T. *Tetrahedron Lett.* **1995**, 36, 9519–9520.
- (a) Ferreira, M. E.; Stoltz, M. B. *J. Am. Chem. Soc.* **2002**, 124, 7726–8202. (b) Mueller, A. J.; Jensen, R. D.; Sigman, S. M. *J. Am. Chem. Soc.* **2002**, 124, 8202–8203. DOI: [10.1021/ja026553m](https://doi.org/10.1021/ja026553m).
- Kantam, M. L.; Ramani, T.; Chakrapani, L.; Choudary, B. M. J. *Mol. Catal. A* **2007**, 274, 11–15. DOI: [10.1016/j.molcata.2007.04.020](https://doi.org/10.1016/j.molcata.2007.04.020).

11. Radosevich, T. A.; Musich, C.; Toste, D. F. *J. Am. Chem. Soc.* **2005**, *127*, 1090–1091. DOI: [10.1021/ja0433424](https://doi.org/10.1021/ja0433424).
12. (a) Arita, S.; Koike, T.; Kayaki, Y.; Ikariya, T. *Angew. Chem.* **2008**, *120*, 2481–2483. (b) Arita, S.; Koike, T.; Kayaki, Y.; Ikariya, T. *Angew. Chem. Int. Ed.* **2008**, *47*, 2447–2449. DOI: [10.1002/ange.200705875](https://doi.org/10.1002/ange.200705875).
13. (a) López, M. C.; Chavant, P. Y.; Molton, F.; Royal, G.; Blandin, V. *ChemistrySelect* **2017**, *2*, 443–450. (b) Alamsetti, S. K.; Mannam, S.; Mutupandi, P.; Sekar, G. *Chem. Eur. J.* **2009**, *15*, 1086–1090.
14. (a) de Wergifosse, M.; Seibert, J.; Grimme, S. *J. Chem. Phys.* **2020**, *153*, 084116. (b) Stephens, P. J., Devlin, F. J. *Chirality* **2000**, *12*, 172–179. (c) Casida, M. E.; Jamorski, C.; Casida, K. C.; Salahub, D. R. *J. Chem. Phys.* **1998**, *108*, 4439–4449. (d) Stratmann, R. E.; Scuseria, G. E.; Frisch, M. J. *J. Chem. Phys.* **1998**, *109*, 8218–8224. (e) Van Caillie, C.; Amos, R. D. *Chem. Phys. Lett.* **2000**, *317*, 159–164.
15. Sheldrick, G. M. *Shelxs-97, Shelxl-97*; Programs for Crystal Structure Analysis, University of Göttingen: Germany, 1997.
16. Altomare, A.; Cascarano, G.; Giacovazzo, C.; Guagliardi, A.; Burla, M. C.; Polidori, G.; Camalli, M. *J. Appl. Crystallogr.* **1994**, *27*, 435–436. DOI: [10.1107/S0021889894000221](https://doi.org/10.1107/S0021889894000221).
17. Betteridge, P. W.; Carruthers, J. R.; Cooper, R. I.; Prout, K.; Watkin, D. J. *J. Appl. Crystallogr.* **2003**, *36*, 1487–1487. DOI: [10.1107/S0021889803021800](https://doi.org/10.1107/S0021889803021800).
18. Frisch, M. J.; Trucks, G. W.; Schlegel, H. B.; Scuseria, G. E.; Robb, M. A.; Cheeseman, J. R.; Scalmani, G.; Barone, V.; Mennucci, B.; Petersson, G. A.; et al. Gaussian, Inc.: Wallingford, CT, 2009.
19. (a) Becke, A. D. *J. Chem. Phys.* **1993**, *98*, 5648–5652. (b) Stephens, P. J.; Devlin, F. J.; Chabalowski, C. F.; Frisch, M. J. *J. Phys. Chem.* **1994**, *98*, 11623–11627. DOI: [10.1063/1.464913](https://doi.org/10.1063/1.464913).
20. (a) Ditchfield, R.; Hehre, W. J.; Pople, J. A. *J. Chem. Phys.* **1971**, *54*, 724. (b) Hehre, W. J.; Ditchfield, R.; Pople, J. A. *J. Chem. Phys.* **1972**, *56*, 2257. (c) Dunning, T. H. Jr. *J. Chem. Phys.* **1989**, *90*, 1007–1023.
21. Scalmani, G.; Frisch, M. J.; Mennucci, B.; Tomasi, J.; Cammi, R.; Barone, V. *J. Chem. Phys.* **2006**, *124*, 1–15. DOI: [10.1063/1.2173258](https://doi.org/10.1063/1.2173258).
22. McKennon, M. J.; Meyers, A. I.; Drauz, K.; Schwarm, M. *J. Org. Chem.* **1993**, *58*, 3568–3571. DOI: [10.1021/jo00065a020](https://doi.org/10.1021/jo00065a020).
23. Gungor, E.; Kara, H.; Colacio, E.; Mota, A. J. *Eur. J. Inorg. Chem.* **2014**, *2014*, 1552–1560. DOI: [10.1002/ejic.201301515](https://doi.org/10.1002/ejic.201301515).
24. Addison, A. W.; Rao, T. N.; Reedijk, J.; Van Rijn, J.; Verschoor, G. C. *J. Chem. Soc. Dalton Trans.* **1984**, 1349–1356. DOI: [10.1039/DT9840001349](https://doi.org/10.1039/DT9840001349).
25. (a) Chopin, N.; Chastanet, G.; Le Guennic, B.; Médebielle, M.; Pilet, G. *Eur. J. Inorg. Chem.* **2012**, 5058–5070. (b) Aronica, C.; Chastanet, G.; Pilet, G.; Le Guennic, B.; Robert, V.; Wernsdorfer, W.; Luneau, D. *Inorg. Chem.* **2007**, *46*, 6108–6119.
26. (a) Farrugia, L. J. *J. Appl. Cryst.* **1999**, *32*, 837–838. (b) Yang, C. T.; Moubaraki, B.; Murray, K. S.; Ranford, J. D.; Vittal, J. J. *Inorg. Chem.* **2001**, *40*, 5934–5941.
27. Nakamoto, K. *Infrared and Raman Spectra of Inorganic and Coordination Compounds*. In *Theory and Applications in Inorganic Chemistry*, 5th ed.; Wiley: New York, 1997.
28. Vogler, A.; Kunkely, H. *Coord. Chem. Rev.* **2007**, *251*, 577–583. DOI: [10.1016/j.ccr.2006.04.015](https://doi.org/10.1016/j.ccr.2006.04.015).
29. Sadhukhan, D.; Ray, A.; Butcher, R. J.; Gómez-García, C. J.; Dede, B.; Mitra, S. *Inorg. Chim. Acta* **2011**, *376*, 245–254. DOI: [10.1016/j.ica.2011.06.024](https://doi.org/10.1016/j.ica.2011.06.024).
30. (a) Enamullah, M.; Chamayou, A.-C.; Banu, K. S.; Kautz, A. C.; Janiak, C. *Inorg. Chim. Acta* **2017**, *464*, 186–194. DOI: [10.1016/j.ica.2017.05.001](https://doi.org/10.1016/j.ica.2017.05.001) (b) Enamullah, M.; Royhan Uddin, A. K. M.; Pescitelli, G.; Berardozi, R.; Makhlofi, G.; Vasylyeva, V.; Chamayoud, A.-C.; Janiak, C. *Dalton Trans.* **2014**, 43, 3313–3329. DOI: [10.1039/C3DT52871E](https://doi.org/10.1039/C3DT52871E) (c) Chamayou, A.-C.; Makhlofi, G.; Nafie, L. A.; Janiak, C.; Lüdeke, S. *Inorg. Chem.* **2015**, *54*, 2193–2203. DOI: [10.1021/ic502661u](https://doi.org/10.1021/ic502661u).
31. Autschbach, J.; Jorge, F. E.; Ziegler, T. *Inorg. Chem.* **2003**, *42*, 2867–2877. DOI: [10.1021/ic020580w](https://doi.org/10.1021/ic020580w).
32. Dünkelfmann, P.; Kolter-Jung, D.; Nitsche, A.; Demir, A. S.; Siegert, P.; Lingen, B.; Baumann, M.; Pohl, M.; Müller, M. *J. Am. Chem. Soc.* **2002**, *124*, 12084–12085. DOI: [10.1021/ja0271476](https://doi.org/10.1021/ja0271476).
33. (a) Enders, D.; Kallfass, U. *Angew. Chem.* **2002**, *114*, 1822–1824. (b) Enders, D.; Kallfass, U. *Angew. Chem. Int. Ed.* **2002**, *41*, 1743–1745. (c) Takikawa, H.; Hachisu, Y.; Bode, W. J.; Suzuki, K. *Angew. Chem.* **2006**, *118*, 3572–3574. (d) Takikawa, H.; Hachisu, Y.; Bode, W. J.; Suzuki, K. *Angew. Chem. Int. Ed.* **2006**, *45*, 3492–3494.
34. Li, Z.; Tang, Z. H.; Hu, X. X.; Xia, C. G. *Chemistry* **2005**, *11*, 1210–1216. DOI: [10.1002/chem.200400818](https://doi.org/10.1002/chem.200400818).